Performance of Protective Barrier for Underground Structures

J.H. Chew and E.C. Leong
School of Civil and Environmental Engineering, Nanyang Technological University, Singapore

ABSTRACT: Underground structures such as service and railway tunnels, pipelines, warehouse and living spaces form an integral part of the infrastructure in our modern society. These underground structures could be subjected to earthquake loading or acts of terrorism. To safeguard human lives and properties, it is important to have a protective system for the underground structures. One possible system is to modify the surrounding ground for the underground structures. This paper investigates the use of different type of materials acting as a protective barrier against ground shock in underground structures numerically. Incident peak pressure was used to examine the efficiency of the protective barrier. From the numerical results, the stiffness of the barrier has a direct impact on the magnitude of the stress wave impacting the structure. Softer material acting as a protective barrier tends to perform better in reducing the propagation of stress waves. Stiffer materials do not fare as well as protective barriers.

1 INTRODUCTION

Underground structures are common in many cities. These underground structures can be service and railway tunnels, pipelines, warehouse, and living spaces. With the increase threat from global terrorism and the advancement of penetrative weapons, there is a need to protect underground structures from ground shock. Damage to underground structures due to ground shock comes from two sources: First, the stress wave from the blast which is the first to arrive, and second, inertial loading cause by the physical movement of the soil block (Davis, 1994). While it is possible to increase the strength of the underground structure (hardening) to resist the damage, it may be more cost effective to use a protective barrier to protect the underground structure. Such a barrier can consist of material of lower density and acoustic impedance than the in-situ soil. Conducting field experiments to study effectiveness of protective barriers on underground structures are costly and time-consuming to perform. Therefore in this study, the effectiveness of different materials acting as the protective barrier was investigated numerically using finite element modelling. The effectiveness of the protective barrier was evaluated based on the incident pressure-time history on the underground structure.

2 DEFINITION OF PROBLEM

A 1.3 kg to 43 kg artillery shell can penetrate into soil to a depth ranging from 0.2m to 8.5m deep (Simms et al., 2004). Many underground structures are sited within this depth. Therefore, the problem studied consists of a structure (8 m length by 5 m width by 6 m height) situated at 2m below the ground surface and extends to a depth of 8m. For a given charge weight, the maximum blast is given by a charge that is fully-coupled with the soil (no cratering) and at the same depth as the mid-point of the structure. Therefore, maximum damage on the structure due to ground shock is at the mid-point of the face of the structure (8 m x 6 m). Based on TM5-855-1 (1986), a charge of 12.64 kg at a burial depth of 5m will not result in cratering. To protect the structure, the barrier must be placed between the blast and the structure. As this barrier is away from the blast (source), it is considered as passive isolation. The distance of the barrier from the structure in this study was arbitrary set at 3.5 m as shown in Fig 1.

3 CHOICE OF FINITE ELEMENT SOFTWARE

There are several finite element software packages that could solve dynamic problems involving explosives. They are namely, LS-DYNA, Autodyn and Abaqus. Similar study on protective barriers have been performed by Wang et al. (2009) using centrifuge tests and numerical modelling using LS-DYNA. They found that the LS-DYNA gave reasonable results. Therefore, LS-DYNA was used in this study.

4 FINITE ELEMENT MODEL

The problem shown in Fig 1 was modelled in three-dimensions using only a quadrant. The quadrant was a 15m cube. The TNT charge was at

4m in front of the barrier. The FE mesh consisted of 66240 eight-noded solid elements with elements ranging in size from 0.125m cube to 0.125m by 0.125m by 0.5m (height) cuboid. The nodes on the lateral boundaries of the model were constrained from lateral movements while the nodes on the bottom boundary were constrained from vertical movements.

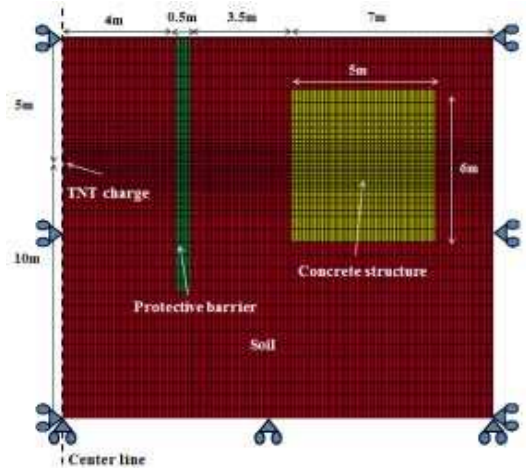

Fig. 1 Side view of finite element model.

Several protective barrier materials were considered. Due to space constraint only six runs consisting of one free-field condition and five types of protective barrier materials (ferrocement, three types of geofoam and an open trench) are presented in this paper. Details of the material models used are presented in the next section. Due to the large distortion of the mesh caused by the explosives, ALE (Arbituary-Lagrangian-Eulerian) formulation was used to perform automatic smoothing and re-zoning of the mesh throughout the simulation.

Only the radial incident pressure on the mid-point of the face of the buried structure is presented to evaluate the effectiveness of the barrier material.

5 MATERIAL MODELS

5.1 *TNT*

In LS-DYNA, MAT_008 (Mat_High Explosive burn) was used to simulate the TNT charge. The TNT properties used were from LLNL explosive handbook (1985). LS-DYNA uses the Jones-Wilkins-Lee (JWL) equation of state (EOS) to model the development of the detonation products gas pressure P:

$$P = A_1\left(1-\omega/R_1V\right)e^{-R_1V} + B_1\left(1-\omega/R_2V\right)e^{-R_2V} + \frac{\omega E_0}{V} \qquad (1)$$

where A1 and B1 are linear coefficients in GPa, R_1, R_2, and ω are nonlinear coefficients, V (= v/v_0) is the relative volume of the detonation products, P is pressure in GPa and lastly, E_0 is the detonation energy per unit volume in kJ/m^3. The parameters for both the TNT and the JWL EOS are summarised in Table 1.

Table 1. Input parameters for TNT and JWL EOS

High explosive burn material – TNT		JWL EOS	
Mass density (kg/m^3)	1630	A_1(GPa)	371.0
		B_1 (GPa)	3.23
Detonation velocity (m/s)	6930	R_1	4.15
		R_2	0.95
Chapman-Jouget pressure (kPa)	2.1e7	ω	0.35
		E_0 (kJ/m^3)	4.35e3
		V (m^3)	1

5.2 *Null model*

The open trench was modeled as air using the null material, MAT_009, in the LS-DYNA material library coupled with the linear polynomial EOS given by the following equation:

$$P = c_0 + c_1\mu + c_2\mu^2 + c_3\mu^3 + (c_4 + c_5\mu + c_6\mu^2)E \qquad (2)$$

where c_0, c_1, c_2, c_3, c_4, c_5 and c_6 are constants that can be defined by the user, μ is the ratio of current density to reference density and E is internal energy. For perfect gas, only c_4 and c_5 are non zero. The input parameters for air are summarised in Table 2.

Table 2. Input parameters for null material

Null properties		Linear polynomial EOS	
Reference density (kg/m^3)	1.025	c_4	0.403
		c_5	0.403

5.3 *Concrete structure model*

The concrete structure was modelled using MAT 078 (Mat-soil concrete). The input parameters for the load curves can be obtained by carrying out triaxial compression test. When under stress, the concrete first deforms elastically (Fig. 2) till it reaches the yield stress which is described by the following yield function ϕ and plotted in Fig. 3:

$$\phi = \sqrt{3J_2} - F(p) \qquad (3)$$

where F(P) is the function of yield stress versus pressure and J_2 is the second invariant of the deviator stress. When there are cracks in the concrete (triggered when strain reaches ε_1), the strength of the concrete is reduced. The strength reduction decreases linearly till it reaches the residual strength (defined by B) at strain ε_2 and remains constant. These two phases were defined

by the curves shown in Fig. 4. The concrete properties used were those suggested by Wang et al. (2008) and are summarised in Table 3.

Table 3. Parameters of concrete

Mass density, ρ (kg/m^3)	2400
Shear modulus, G (kPa)	4.5e5
Bulk modulus, K (kPa)	6e5
Tension cutoff, PC (kPa)	-2e3
Residual strength factor, B	0.3

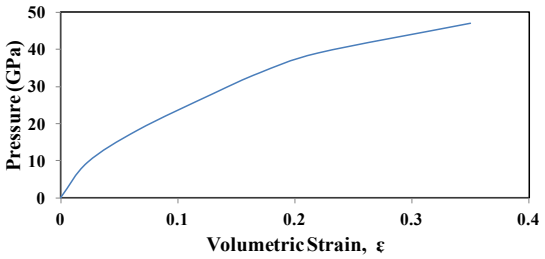

Fig. 2 Pressure vs volumetric strain.

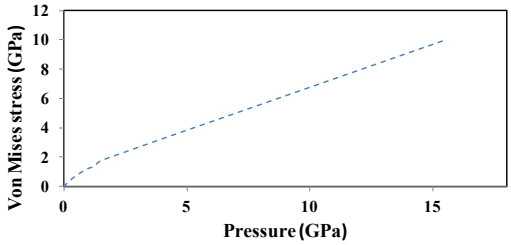

Fig 3. Von Mises stress vs pressure.

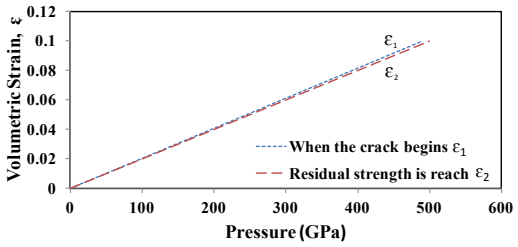

Fig. 4 Volumetric strain vs pressure when crack begins.

5.4 *Soil and foam model*

Krieg (1972) created a soil and foam model, MAT_005, in LS-DYNA to simulate an elastic-plastic material. The yield function of the model ϕ is described by the following equation:

$$\phi = J_2 - (a_0 + a_1 p + a_2 p^2) \quad (4)$$

where p is the pressure, a_0, a_1 and a_2 are constants, and J_2 is the second invariant of the deviator stress. Initially, the model is linearly elastic at small strains under tension or compression and becomes nonlinear at higher strain levels. The soil, ferrocement and geofoam were modelled using this material model. The soil was modelled with c' = 1.3 kPa and ϕ' = 28°. The mass density, shear modulus and bulk modulus of the soil were chosen to simulate sandy loam/dry sand. The material properties of ferrocement were obtained from Lin et al. (2010) and the geofoam properties were obtained from AFM Corporation (2014). The material properties for soil (S), ferrocement (FC), and Geofoams A, B and C (GA, GB and GC, respectively) are summarised in Table 4.

Table 4. Soil, ferrocement and foam properties

	S	GA	GB	GC	FC
ρ (kg/m^3)	1800	11.2	21.6	45.7	2400
G (kPa)	1.6e4	6.7e2	2.2e3	5.71e3	7.98e3
K (kPa)	4.9e4	6.6e2	2.2e3	5.61e3	1.27e4
PC (kPa)	-3.9	-69	-240	-517	-2.6e3
a_0	2.4e6	0	0	0	2.5e10
a_1	2.2e3	0	0	0	0
a_2	0.48	0.35	0.35	0.35	0

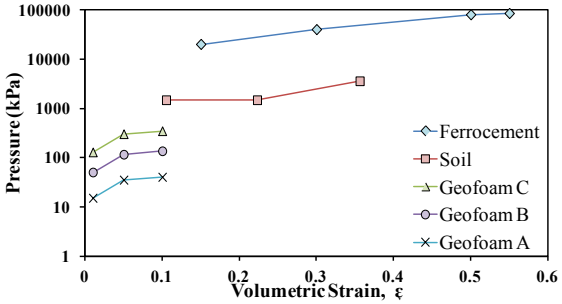

Fig. 5 Pressure vs volumetric strain.

6 FE MODEL VERIFICATION

To verify that the FE model performed correctly, it was first used to simulate a free-field explosion (without protective barrier and buried structure). The peak pressures at distances of 10 and 15m away from the charge were plotted in the dimensionless peak pressure plot of Leong et al. (2007) in Fig. 6. The results showed good agreement with the line describing sandy loam/ dry sand as shown in Fig. 6. This shows that the FE model provided the correct free-field peak pressures.

7 RESULTS AND DISCUSSIONS

The radial pressure-time histories at mid-point of the face of the structure are plotted in Fig. 7 for no barrier, ferrocement barrier, geofoam barriers and open trench. Fig. 7 shows that geofoams were more effective than ferrocement in reducing the peak incident pressure on the structure. However, Geofoam A showed that the pressure persisted over a much longer time than Geofoams B and C. Fig. 7 shows that the open trench was the most effective barrier in reducing the incident peak

pressure on the structure. The percentages of peak pressure reduction for each type of the barrier relative to the no-barrier condition are also shown in legend of Fig. 7.

The arrival time of the blast wave at the structure differs with the type of the barrier material used. The difference in arrival times is clearly shown when comparing the arrival times between ferrocement and Geofoam A. The ferrocement barrier gave a faster arrival time. The difference in arrival times will increase as the thickness of the barrier increases.

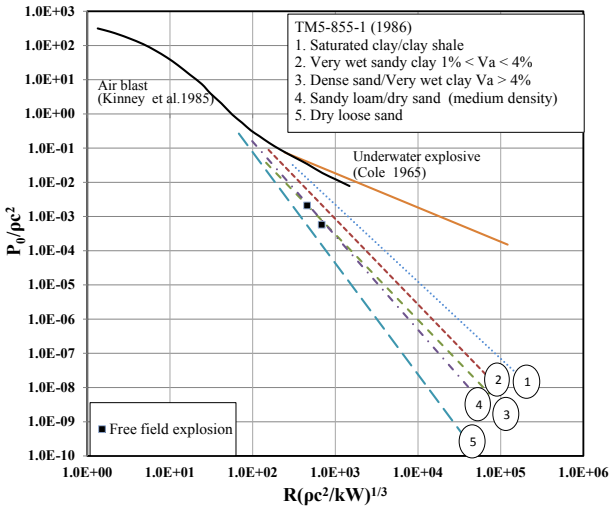

Fig. 6 Dimensionless peak pressure versus scaled distance plot (modified from Leong et al. 2007).

8 CONCLUSIONS

Field experiments to determine effectiveness of protective barrier for underground structures are costly and time-consuming to perform. Therefore, numerical modelling provides a reasonable alternative. In this study, the effectiveness of ferrocement, geofoam and an open trench as a protective barrier for underground structure against ground shock was investigated numerically using LS-DYNA. The open trench was found to be the most effective while ferrocement was found to be the least effective. In summary, incident peak pressure on structure reduces and arrival time at the structure increases as the stiffness of the barrier material reduces. Considering the practical difficulty of using an open trench as a protective barrier, a low density geofoam appears to be a good alternative. Further studies on effects of varying the dimension of the protective barrier and its distance from the structure to be protected will be performed in the near future.

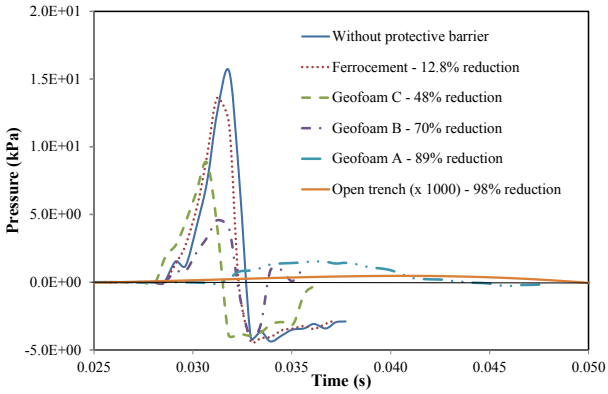

Fig. 7 Pressure-time history plot for free-field, ferrocement and geofoam.

ACKNOWLEDGEMENTS

The first author acknowledges the research scholarship from Nanyang Technological University, Singapore. The financial support from grant MINDEF-NTU-JPP/13/01/02 administered by the Protective Technology Research Center, Nanyang Technological University, is gratefully acknowledged.

REFERENCES

AFM Corporation (2014). Foam control EPS geofoam tech data. <http://www.geofoam.com> (Oct. 1, 2014).

Davies, M.C.R., (1994). Dynamic soil structure interaction resulting from blast loading, Proceedings of the International Conference Centrifuge, Singapore, pp. 319-324.

Krieg, R. D. (1972). A simple constitutive description for cellular concrete. Sandia Report SC-DR-72-0883.

Leong, E.C., Anand, S., Cheong, H.K. and Lim, C.H. (2006). Re-examination of peak stress and scaled distance due to ground shock. International Journal of Impact Engineering, 34(9): 1487-1499.

Lin, V.W.J., Quek, S.T., Maalej, M., and Lee, S.C., (2010). Finite element model of functionally-graded cementitious panel under small projectile impact. International Journal of Protective Structure, 1:271-297.

LLNL (1985). Explosive Handbook - Properties of Chemical Explosives and Explosive Simulants, University of California, Livermore.

LSTC (2006) LS-DYNA Theory Manual, Livermore Software Technology Corporation, California, USA.

Simms, J.E., Larson, R.J, Murphy, W.L., and Butler, D.K., (2004). Guidelines for Planning Unexploded Ordnance (UXO) Detection Surveys. US Army Corps of Engineers, Research and Development Center.

TM5-855-1 (1986). Fundamentals of Protective Design for Conventional Weapons, Department of Army, Washington DC, USA.

Wang, J.G., Sun, W., and Anand, S., (2009). Numerical investigation on active isolation of ground shock by soft porous layers. Journal of Sound and Vibration, 321:492-509.